
Fractal Graph Contrastive Learning

Nero Z. Li*

Department of Mathematics
Imperial College London
University of Oxford
ziyu.li21@imperial.ac.uk

Xuehao Zhai*

Department of Civil and Environmental Engineering
Imperial College London
x.zhai20@imperial.ac.uk

Zhichao Shi

School of Advanced Interdisciplinary Sciences
University of Chinese Academy of Sciences
State Key Lab of AI Safety, Institute of Computing Technology
Chinese Academy of Sciences
shizhichao22@mails.ucas.ac.cn

Boshen Shi

China Mobile Research Institute
boshenshi97@gmail.com

Xuhui Jiang[†]

DataArc Tech Ltd.
IDEA Research International Digital Economy Academy
jiangxuhui@idea.edu.cn

Abstract

While Graph Contrastive Learning (GCL) has attracted considerable attention in the field of graph self-supervised learning, its performance heavily relies on data augmentations that are expected to generate semantically consistent positive pairs. Existing strategies typically resort to random perturbations or local structure preservation, yet lack explicit control over global structural consistency between augmented views. To address this limitation, we propose Fractal Graph Contrastive Learning (FractalGCL), a theory-driven framework that leverages fractal self-similarity to enforce global topological coherence. FractalGCL introduces two key innovations: a renormalisation-based augmentation that generates structurally aligned positive views via box coverings; and a fractal-dimension-aware contrastive loss that aligns graph embeddings according to their fractal dimensions. While combining the two innovations markedly boosts graph-representation quality, it also adds non-trivial computational overhead. To mitigate the computational overhead of fractal dimension estimation, we derive a one-shot estimator by proving that the dimension discrepancy between original and renormalised graphs converges weakly to a centred Gaussian distribution. This theoretical insight enables a reduction in dimension computation cost by an order of magnitude, cutting overall training time by approximately 61%. The experiments show that FractalGCL not only delivers state-of-the-art results on standard benchmarks but also outperforms traditional baselines on traffic networks by an average margin of about remarkably 7%. Codes are available at (<https://anonymous.4open.science/r/FractalGCL-0511/>).

*equal contribution

[†]corresponding author

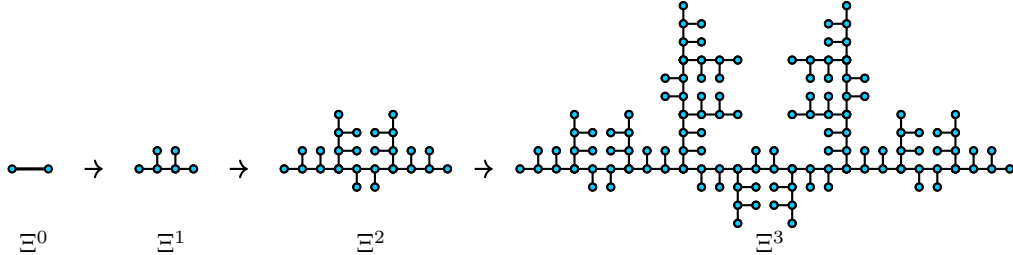


Figure 1: An example of evolving theoretical fractal graph [26]

1 Introduction

Graph contrastive learning (GCL) has emerged as a popular self-supervised paradigm for graph representation learning [8, 40, 44, 13, 20, 43]. By forcing models to discriminate positive pairs from negative pairs, it alleviates the knowledge scarcity problems [39, 42, 2, 31], and it also serves as an effective pretext task for pre-training graph foundation models [19, 9]. As graphs possess non-Euclidean topology, researchers must tailor contrastive learning frameworks to graph-specific properties. Therefore, GCL has formed unique lines of research, which cover stages including augmenting graph data [21, 30, 34], designing contrastive modes [12, 29, 27], and optimizing contrastive objectives [6, 41, 48].

Among current studies, data augmentation remains a pivotal challenge in graph contrastive learning, as the quality of positive and negative sample pairs fundamentally determines the capacity of a graph model to extract meaningful knowledge and the quality of learned representations. While negative samples are typically generated by contrasting views from structurally distinct graphs or subgraphs [46], which ensures divergent distributional characteristics, the generation of semantically coherent positive samples remains a critical bottleneck. Specifically, existing approaches often rely on random perturbations (e.g., node/edge deletion, attribute masking) or fixed topological constraints (e.g., hierarchy preservation), which provide only incomplete guarantees for maintaining structural consistency. These methods lack an explicit mechanism to ensure global similarity between the original graph and its augmented views, leading to potential mismatches in semantic alignment. This gap naturally raises a fundamental question: *Can we design a principled graph-level criterion to enforce global structural consistency during positive sample generation?*

This critical question directs attention to a fundamental yet often overlooked global property of graphs—their inherent self-similarity and hierarchical complexity, which is mathematically formalised through the concept of **fractal**. Fractal geometry [3, 22, 23] is a field of mathematics that explores irregular shapes whose intricate detail persists across different scales, appearing in patterns such as snowflakes, coastlines, and branching trees. Fractal graphs are networks that possess fractal properties, effectively transplanting fractal concepts from Euclidean space onto graph structures (see Figure 1). Given the prevalence of fractal graphs in natural and society, their fractal properties likely play a significant yet under-explored role in improving graph representations via GCL.

To effectively utilize fractal properties, we propose a novel FractalGCL framework in this paper, improving the effectiveness of GCL. We start by introducing a novel augmentation strategy, **renormalisation**, to generate positive views which are structurally similar. Therefore, the generated views have the same box dimension, implying strong structural similarity. To ensure that the graph representations capture not only self-similar structures but also explicitly encode fractal-dimension information, we define a **fractal-dimension-aware contrastive loss** that steers the encoder to embed graphs in a way that respects their intrinsic fractal geometry. Empirically, the two components already outperform competing models, yet estimating the fractal dimension introduces additional computational overhead. Consequently, we cut the cost of box-dimension estimation with a theoretical result that approximates the dimension gap as a **Gaussian perturbation**, making FractalGCL practical and performant. Experiments were conducted on both standard graph classification benchmarks and real-world traffic networks, and the results confirm that FractalGCL surpasses prior methods on most individual benchmarks and attains the best average performance overall, underscoring its effectiveness in both theory and practice.

To sum up, our main contributions include:

- **Fractal Geometry Meets GCL.** To the best of our knowledge, we are among the first to inject a mathematically rigorous fractal viewpoint into graph representation learning and graph contrastive learning, revealing that a global and scale-free structure, which is often overlooked by prior GCL methods, demonstrates significant potential in learning high-quality graph representations and enhancing performance on downstream tasks.
- **Theory-Driven FractalGCL Architecture.** Guided by fractal geometry, we improve the existing GCL methods with a novel framework FractalGCL. It integrates renormalisation-based graph augmentations and a fractal-dimension-aware contrastive loss. Renormalisation contributes to generating better positive and negative pairs, while the novel loss further utilizes fractal property to optimize graph embeddings.
- **From Theory to Implementation.** To further optimize Fractal GCL for practical implementation, we conducted a series of theoretical analyses to prove that the gap between the original and renormalised box dimensions converges weakly to a centred Gaussian measure, enabling a lightweight approach that markedly accelerates training.
- **Notable Performance Gains.** We conducted thorough experiments on both standard graph classification benchmarks and social datasets, such as urban-traffic graphs, and the results prove the effectiveness of the proposed FractalGCL.

2 Preliminary Experiments

The foregoing discussion can be condensed into two working hypotheses: **(i)** fractal structures are widespread in real-world graphs, and **(ii)** such patterns reflect non-trivial global complexity that may influence representation learning.

We now present two preliminary studies to investigate these questions. *Preliminary experiment 1* measures how often strong fractality occurs in standard benchmarks, and *Preliminary experiment 2* evaluates whether explicitly using fractal information can boost downstream performance. Please refer to Appendix B for the detailed experimental setup and complete results.

Preliminary experiment 1 We assessed how well each graph in six graph classification benchmarks follows fractal (power-law) scaling by fitting a log–log box-counting linear regression and recording its **coefficient of determination** R^2 : the closer R^2 is to 1, the more convincingly the graph is fractal.

Using the strict cutoff $R^2 \geq 0.90$, 81% of the PROTEINS graphs, 92% of the REDDIT-MULTI-5K graphs, and an impressive 99.8% of the D&D graphs meet the criterion and similarly high ratios on the remaining datasets; see Figure 2. Hence, strongly fractal graphs are not rare outliers but a pervasive phenomenon across all six collections.

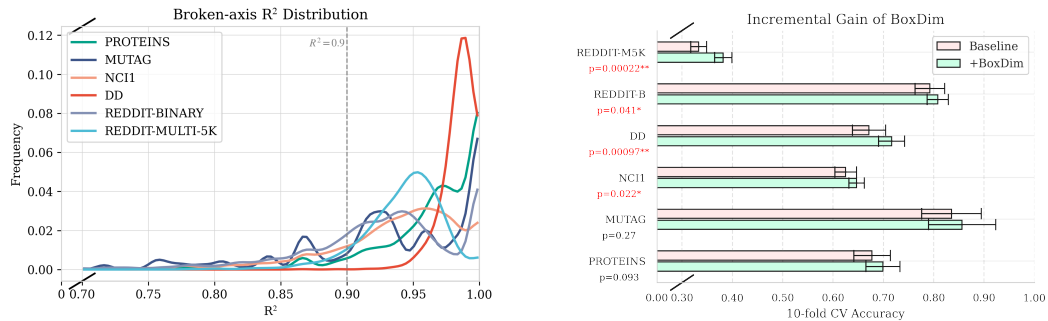


Figure 2: Prevalence of fractal structures

Figure 3: Accuracy gains from adding box dimension (significant when $p < 0.05$)

Preliminary experiment 2 We augmented a new feature **box dimension**, a type of fractal dimension introduced in Section 3.1, to original features in each benchmark, and report the difference in classification accuracy before and after augmentation. Remarkably, four out of six benchmarks show *statistically significant* gains ($p < 0.05$), strongly indicating that fractal information captures

unique topological features that previous models fail to capture. Besides, the largest improvement ($p = 9.7 \times 10^{-4}$) appears on the most fractal and large-scale graphs, suggesting that box dimension is especially informative when global self-similarity is pronounced.

3 FractalGCL: Theory, Methodology and Implementation

This section constructs FractalGCL—a novel framework grounded in fractal geometry that enables graph representations to capture global fractal structure and box dimension information at the graph level. Specifically, Section 3.1 revisits the essentials of fractal geometry; Sections 3.2–3.3 present our renormalisation-based augmentations and the accompanying dimension-aware contrastive loss, which form core components in FractalGCL framework; However, computing the fractal loss for each renormalised graph is extremely costly. Sections 3.4–3.5 address the resulting computational challenge by mathematical proof and statistical analysis and detail the practical implementation of FractalGCL. See Figure 4 for intuitive ideas.

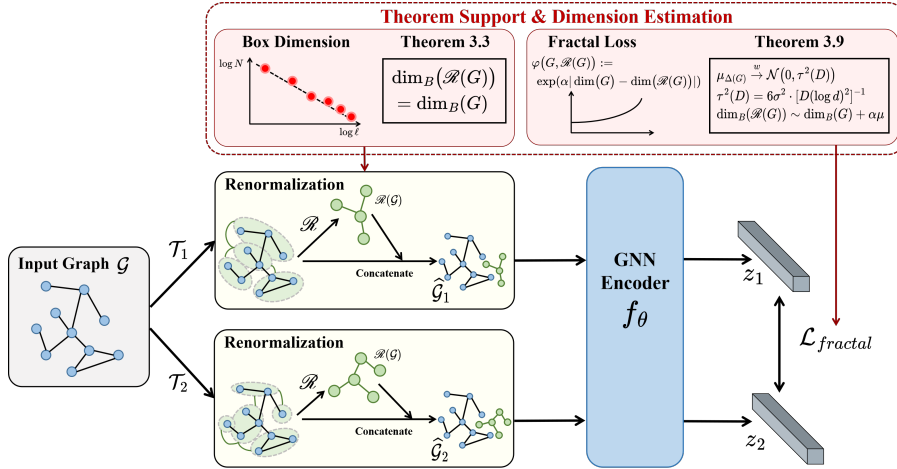


Figure 4: The Pipeline of FractalGCL

3.1 Background of Fractal Geometry

In mathematics, defining a fractal graph is far from straightforward. However, to keep the discussion focused, we state the most practical definition of fractal dimension in plain terms here, leaving the full technical treatment to Appendix A.

Definition 3.1. Let G be an infinite graph equipped with the graph distance d_G . An L box covering of G is a collection of subgraphs $\{U_i\}_{i \in \mathcal{I}}$, indexed by \mathcal{I} , such that $\bigcup_{i \in \mathcal{I}} U_i = G$, and $\text{diam}(U_i) \leq L$ for any $i \in \mathcal{I}$. Denote by $N_L(G)$ the minimum number of subgraphs required for an L box covering of G . The **Minkowski dimension** (or **box dimension**) of G is then defined as

$$\dim_B(G) := \lim_{L / \text{diam}(G) \rightarrow 0} \frac{\log N_L(G)}{-\log(L / \text{diam}(G))},$$

provided the limit exists. If $0 < \dim_B(G) < \infty$, we say that G exhibits a fractal property and call G a fractal (Minkowski) graph.

To estimate the fractal dimension of a finite graph in practice, we design the algorithm estimating the box dimension. It forms the basis on which FractalGCL is built. Find full details on the box dimension algorithm in Appendix A.

3.2 New Augmentation: Graph Renormalisation

In this section, we first formally introduce the renormalised graph $\mathcal{R}(G)$ and highlight its distinctive value when used as a novel augmentation in contrastive learning. We then present theoretical results showing that the renormalisation procedure preserves the fractal dimension of a graph, thereby providing a solid analytical foundation for our approach.

Renormalisation Graph In contrastive learning, constructing an “augmented graph” that retains structural similarity while preserving appropriate differences from the original is crucial. Here, we introduce the concept of the *renormalisation graph*, whose core idea has appeared in various literature (e.g., in multi-scale network analysis and abstractions of complex networks [32]), but whose application to augmentations for contrastive learning is relatively novel.

Definition 3.2. Let G be a given graph, and let $\{U_i\}_{i \in \mathcal{I}}$ be an L box-covering of G . We construct the renormalised graph $\mathcal{R}(G)$ as follows: (i) Collapse each covering set U_i into a single supervertex v_i . (ii) If there exists at least one edge in G connecting a vertex in U_i to a vertex in U_j (with $i \neq j$), then place a superedge between v_i and v_j in $\mathcal{R}(G)$.

The resulting graph $\mathcal{R}(G)$ is called the renormalised graph of G at the given scale L .

From an intuitive standpoint, the construction of $\mathcal{R}(G)$ disregards certain fine-grained local structures while highlighting the global characteristics of the original graph in a more compact form. Because renormalisation at different scales can accentuate multi-scale self-similarity, having both G and $\mathcal{R}(G)$ simultaneously in contrastive learning allows the model to “perceive” macro-level structural resemblance, thereby facilitating a more effective capture of the essential features of a fractal network. Full algorithmic details are deferred to Appendix A.

Theorem 3.3. For any Minkowski (box-dimensional) graph G , mathematically,

$$\dim_B(\mathcal{R}(G)) = \dim_B(G).$$

Proof. See Theorem A.2 in Appendix. □

Theorem 3.3 formally states that the box dimension is invariant under renormalisation, ensuring that $\mathcal{R}(G)$ and G share the same intrinsic fractal complexity.

In experimental practice, we construct the augmentation view as the disjoint union $G \sqcup \mathcal{R}(G)$. Because $\mathcal{R}(G)$ preserves both the fractal dimension and the self-similar structure of G , it serves as a scaled-down fractal module drawn from the same generative process. Appending this module to G enlarges the global pattern while introducing controlled local variation, producing an augmented graph that is recognizably similar yet still distinguishable from the original. See Figure 4.

3.3 Novel Loss: Fractal-Dimension Based

While renormalisation already captures the fractal structure, in this section we introduce a contrastive loss with fractal dimension. Together, these components yield a graph representation learning framework that embeds each graph’s fractal characteristics.

Mapping from Graph G to Representation \mathbf{z} we apply \mathcal{R} to obtain the augmented graph $\mathcal{R}(G_n)$. We then use a GNN-based encoder $f_\theta(\cdot)$ and a readout function $\text{Readout}(\cdot)$ to produce a graph-level embedding, and finally apply a projection head $g_\phi(\cdot)$ to map it into the contrastive space: $\mathbf{z}_n := g_\phi(\text{Readout}(f_\theta(\mathcal{R}(G_n))))$.

Contrastive Loss with Fractal Weight We define the fractal dimension discrepancy weight between G_n and its augmented version $\mathcal{R}(G_n)$ as

$$\varphi(G_n, \mathcal{R}(G_n)) := \exp(\alpha |\dim_B(G_n) - \dim_B(\mathcal{R}(G_n))|),$$

where $\dim_B(\cdot)$ denotes the (estimated) fractal dimension of a graph, and $\alpha \geq 0$ is a scaling factor.

Assume we have N original graphs $\{G_n\}_{n=1}^N$ in a minibatch. Each G_n is augmented to produce $(G_n, \mathcal{R}(G_n))$, yielding representations \mathbf{z}_n and $\mathbf{z}_n^{(\mathcal{R})}$, respectively. We treat $(\mathbf{z}_n, \mathbf{z}_n^{(\mathcal{R})})$ as a *positive*

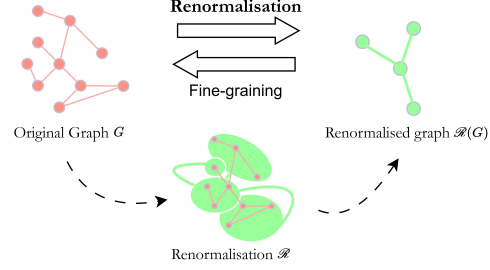


Figure 5: Graph Renormalisation

pair in the spirit of contrastive learning, while representations from other graphs in the batch serve as *negative* examples. An InfoNCE-like loss with the fractal dimension weight is given by:

$$\ell_{\text{fractal}}(n) := -\log \frac{\exp\left(\text{sim}(\mathbf{z}_n, \mathbf{z}_n^{(\mathcal{R})})/\tau\right) \cdot \varphi(G_n, \mathcal{R}(G_n))}{\sum_{n'=1, n' \neq n}^N \exp\left(\text{sim}(\mathbf{z}_n, \mathbf{z}_{n'})/\tau\right) \cdot \varphi(\mathcal{R}(G_n), \mathcal{R}'(G_{n'}))}.$$

We average over all n to obtain the overall *fractal contrastive loss*: $\mathcal{L}_{\text{fractal}} := \frac{1}{N} \sum_{n=1}^N \ell_{\text{fractal}}(n)$.

Lemma 3.4. *Denote the similarity by $s := \text{sim}(\mathbf{z}_G, \mathbf{z}_{\mathcal{R}(G)})$. Keeping all other batch terms fixed, the fractal-weighted InfoNCE loss ℓ_{fractal} satisfies*

$$\left| \partial \ell_{\text{fractal}} / \partial s \right| = w \left| \partial \ell_{\text{InfoNCE}} / \partial s \right|, w = \exp(\alpha \Delta) \text{ increases strictly with } \Delta.$$

Proof. Straightforward by partial differentiation. \square

Intuitively, a larger fractal-dimension gap Δ amplifies the positive-pair gradient, forcing the model to pull the two views closer, while $\Delta = 0$ reduces to the ordinary InfoNCE case. The lemma therefore formalises how the weight $\exp(\alpha \Delta)$ adaptively injects fractal similarity into the optimisation dynamics.

Proposition 3.5 (Dimension–Dominated Ranking Consistency). *If $\Delta_1 < \Delta_2$ and $s_1 - s_2 \leq \tau \alpha(\Delta_2 - \Delta_1)$, then the fractal-weighted InfoNCE losses satisfy*

$$\ell_{\text{fractal}}(G, H_2) < \ell_{\text{fractal}}(G, H_1).$$

Proof. See Appendix A.3. \square

Proposition 3.5 shows that when two candidates have nearly identical embedding similarities, the fractal-weighted InfoNCE loss favours the one whose fractal dimension is closer to that of the anchor graph, ensuring that fractal characteristics dominate the loss’s discriminative behaviour.

3.4 Computational Dilemma and Its Solution

In practice, the renormalisation augmentation combined with the fractal-dimension loss already yields strong downstream performance, but computing that loss for every renormalised graph is computationally expensive. This section analyzes the bottleneck and presents an efficient remedy.

To conclude, in practice we encounter the following dilemma:

- (I) Simply imposing equal dimensions before and after renormalisation by Theorem 3.3, as guaranteed asymptotically by the theorem, overlooks the discrepancies that arise in finite graphs.
- (II) Conversely, computing the fractal dimension for every augmented graph is prohibitively complex. The following Proposition 3.6 indicates that the per-augmentation estimation is unrealistic.

Proposition 3.6 (Fractal complexity on sparse graphs). *For the greedy box-covering procedure in Algorithm 3, the worst-case running time $T(V)$ obeys*

$$\Omega(V^2) \leq T(V) \leq O(V^3).$$

Proof. See Appendix A.4. \square

Hence, to make fractal-based graph embeddings more broadly applicable, we must pursue *faster* or *approximate* methods to estimate box dimensions. In the following, we propose a statistical approximation strategy that circumvents the high computational overhead of naive box-covering, thereby enabling the fractal-weighted contrastive learning framework to scale to larger graphs and more frequent augmentations.

A Theoretical Solution to the Dimension Dilemma We avoid the heavy cost of recomputing $\dim(\mathcal{R}(G))$ at every augmentation step by modelling the finite-size deviation $\Delta(G) := \dim(G) - \dim(\mathcal{R}(G))$ as a random perturbation whose variance vanishes as the graph grows. The argument proceeds in three succinct steps.

Step 1. Finite-diameter error magnitude. Let G be a graph with diameter $D := \text{diam}(G)$. Write \hat{m}_G for the OLS slope used to estimate $\dim(G)$ and σ^2 for the log-residual variance.

Lemma 3.7 (Standard error vs. diameter). *For any graph G , $\text{SE}(\hat{m}_G) \sim \sqrt{6} \sigma [\sqrt{D} \log D]^{-1}$.*

Proof. See Appendix A.5. □

Lemma 3.7 quantifies how rapidly the slope uncertainty shrinks: the error decays as $1/(\sqrt{D} \log D)$.

Step 2. Asymptotic distribution of the slope.

Lemma 3.8. *Under Assumptions (A1)–(A4),*

$$\sqrt{D} (\hat{m}_G - m_G) \xrightarrow{\mathcal{D}} \mathcal{N}(0, \sigma^2), \quad \sqrt{D} (\hat{m}_{\mathcal{R}} - m_{\mathcal{R}}) \rightarrow \mathcal{N}(0, \sigma^2).$$

Proof. Immediate from the classical OLS central-limit theorem. □

Lemma 3.8 states that, once rescaled by \sqrt{D} , the slope estimator for either graph becomes asymptotically Gaussian with a diameter-independent variance σ^2 . Hence any finite-size fluctuation of the estimated dimension is fully captured by a normal term whose magnitude is controlled only by D .

Step 3. Weak convergence of the dimension gap.

Theorem 3.9. *Let μ_G be the probability measure induced by the random variable $\Delta(G) = \dim(G) - \dim(\mathcal{R}(G))$ on a graph G . Under Hypothesis A.6 and with the notation of Lemmas 3.7 and 3.8, we have*

$$\mu_G \xrightarrow{w} \mathcal{N}(0, \tau^2(D)), \quad \tau^2(D) = 6\sigma^2 [D(\log D)^2]^{-1},$$

as $D \rightarrow \infty$. In particular, $\tau^2(D) \rightarrow 0$, so the limiting distribution degenerates to the Dirac measure δ_0 ; i.e. $\Delta(G) \rightarrow 0$ in probability.

Proof. See Appendix A.7. □

Corollary 3.10. *When $D \rightarrow \infty$ the variance $\tau^2(D)$ vanishes and $\mu_G \rightarrow \delta_0$, so $\dim(G) = \dim(\mathcal{R}(G))$ with probability 1 in the infinite-diameter limit.*

Summary. Accordingly, we estimate the renormalised graph's dimension for *every* G by adding a zero-mean Gaussian perturbation with this scale, rather than rerunning the full box-covering procedure. This scale-adaptive stochastic perturbation preserves fractal information while replacing the prohibitive deterministic computation with an analytically grounded, lightweight approximation.

3.5 Practical Implementation

In this section, we integrate the newly developed methods and theory to implement the FractalGCL.

Loss approximation. For a minibatch $\{G_1, \dots, G_N\}$ we draw independent perturbations

$$\mu_n \sim \mathcal{N}(0, \tau^2(D_n)), \quad \nu_{nk} \sim \mathcal{N}(|\dim(G_n) - \dim(G_k)|, \tau^2(D_n) + \tau^2(D_k)),$$

where $D_n = \text{diam}(G_n)$ and $\hat{\sigma} \approx 0.1$ is the pilot-estimated residual scale. The fractal loss then reads $\ell_n^{\text{fractal}} = -\log \frac{\exp(\text{sim}(\mathbf{z}_n, \mathbf{z}_n^{(\mathcal{R})})/\tau + \alpha\mu_n)}{\sum_{k \neq n} \exp(\text{sim}(\mathbf{z}_n, \mathbf{z}_k^{(\mathcal{R})})/\tau + \alpha\nu_{nk})}$.

Implementation details. During training we first compute (or cache) each graph diameter D_i , then form the similarity matrix $\mathbf{S} = [\text{sim}(\mathbf{z}_i, \mathbf{z}_j^{(\mathcal{R})})]$ and augment it with a Gaussian matrix whose entrywise statistics obey the diameter-controlled variance above:

$$\mathbf{S}^* = \mathbf{S} + \alpha \mathbf{G}, \quad \mathbf{G}_{ij} \sim \begin{cases} \mathcal{N}(0, \tau^2(D_i)), & i = j, \\ \mathcal{N}(|\dim(G_i) - \dim(G_j)|, \tau^2(D_i) + \tau^2(D_j)), & i \neq j. \end{cases}$$

An annealing schedule on $\hat{\sigma}$ (or directly on α) keeps the injected noise large in early epochs and negligible later. Softmax over \mathbf{S}^* yields the final fractal-weighted contrastive loss, adding only at almost the $\mathcal{O}(N^2)$ cost of sampling \mathbf{G} to each batch.

4 Experiments

4.1 Setup

We validate FractalGCL on unsupervised representation learning tasks using six widely-adopted datasets from TUDataset [24]: NCI1, MUTAG, PROTEINS, D&D, REDDIT-BINARY(REDDIT-B), and REDDIT-MULTI-5K(REDDIT-M5K). We adopt a 2-layer GIN as the encoder, and a sum pooling is used as the readout function; renormalisation adopts greedy box-covering with radius 1, dimension weight $\alpha = 0.1$, and temperature $\tau = 0.4$. Models are first trained with Adam on the unlabeled data only. After that, a non-linear SVM classifier is used to evaluate the graph representations. Accuracy is reported under 10-fold cross-validation. The experiments are repeated 5 times to report the mean and standard deviation. We conduct our experiments on an Ubuntu machine with one 40GB NVIDIA A100 GPU.

4.2 Main Results

Table 1: Classification accuracy on benchmark datasets (10-fold CV).

Model	NCI1	MUTAG	PROTEINS	D&D	REDDIT-B	REDDIT-M5K	AVG.
GAE [14]	74.36 \pm 0.24	72.87 \pm 6.84	70.51 \pm 0.17	74.54 \pm 0.68	87.69 \pm 0.40	33.58 \pm 0.13	68.93
graph2vec [25]	73.22 \pm 1.81	83.15 \pm 9.25	73.30 \pm 2.05	70.32 \pm 2.32	75.48 \pm 1.03	47.86 \pm 0.26	70.56
DGI [35]	74.86 \pm 0.26	66.49 \pm 2.28	72.27 \pm 0.40	75.78 \pm 0.34	88.66 \pm 0.95	53.61 \pm 0.31	71.95
InfoGraph [33]	76.20 \pm 1.06	89.01 \pm 1.13	74.44 \pm 0.31	72.85 \pm 1.78	82.50 \pm 1.42	53.46 \pm 1.03	74.74
GraphCL [46]	77.87 \pm 0.41	86.80 \pm 1.34	74.39 \pm 0.45	78.62 \pm 0.40	89.53 \pm 0.84	55.99 \pm 0.28	77.20
ContextPred [7]	73.00 \pm 0.30	71.75 \pm 7.34	70.23 \pm 0.63	74.66 \pm 0.51	84.76 \pm 0.52	51.23 \pm 0.84	70.94
JOAO [45]	78.07 \pm 0.47	87.35 \pm 1.02	74.55 \pm 0.41	77.32 \pm 0.54	85.29 \pm 1.35	55.74 \pm 0.63	76.39
JOAOv2 [45]	78.36 \pm 0.53	87.67 \pm 0.79	74.07 \pm 1.10	77.40 \pm 1.15	86.42 \pm 1.45	56.03 \pm 0.27	76.66
SimGRACE [40]	79.12 \pm 0.44	89.01 \pm 1.31	74.03 \pm 0.09	77.44 \pm 1.11	89.51 \pm 0.89	55.91 \pm 0.34	77.50
RGCL [17]	78.14 \pm 1.08	87.66 \pm 1.01	75.03 \pm 0.43	78.86 \pm 0.48	90.34 \pm 0.58	56.38 \pm 0.40	77.74
DRGCL [10]	78.70 \pm 0.40	89.50 \pm 0.60	75.20 \pm 0.60	78.40 \pm 0.70	90.80 \pm 0.30	56.30 \pm 0.20	78.15
GradGCL [16]	79.72 \pm 0.53	88.46 \pm 0.98	74.89 \pm 0.39	78.95 \pm 0.47	90.45 \pm 1.06	56.20 \pm 0.31	78.11
FractalGCL	80.50 \pm 0.16	91.71 \pm 0.23	75.85 \pm 0.40	80.14 \pm 0.12	88.13 \pm 0.13	56.45 \pm 0.14	78.80

Table 1 reports the accuracy of the downstream graph classification task on six benchmark datasets. FractalGCL achieves the highest average score (**78.80%**), outperforming the strongest baseline (GradGCL, 78.11%) by **0.69 pp**. It ranks first on five of the six datasets—**NCI1, MUTAG, PROTEINS, D&D, and REDDIT-MULTI-5K**. The most strongly fractal benchmark D&D exhibits a big margin (+1.19 pp), which is consistent with our hypothesis that fractal-aware augmentations and loss provide greater benefit when the underlying graphs display pronounced self-similarity. These results confirm that injecting the fractal structure into a graph contrastive learning not only matches but often exceeds the performance of carefully tuned augmentation-based methods, while retaining the same encoder capacity and training budget. It is worth noting that FractalGCL performs noticeably worse on the Reddit-Binary dataset. This dataset contains the lowest proportion of strongly fractal graphs among all six benchmarks (see Appendix A), which aligns with the theoretical expectation that our method excels when fractal structure is prevalent.

4.3 Evaluation on Practical Scenarios

To assess the real-world applicability of FractalGCL, we followed network collection way in [47] to construct urban road graphs for Chicago, New York and San Francisco. We then randomly sampled

square sub-graphs from each complete road network. The downstream task predicts the traffic-accident severity of each area, following [49]. Full experimental details and results are provided in Appendix B.

Table 2: Classification accuracy on traffic tasks.

Task	City	DGI	InfoGraph	GCL	JOAO	SimGRACE	FractalGCL
total_accidents_high	Chicago	54.91±10.75	56.54±11.85	63.12±13.36	55.86±12.21	62.75±13.50	64.60±13.32
	SF	76.45±14.47	78.74±13.60	80.06±13.32	79.75±13.61	80.40±13.47	80.89±12.92
	NY	51.51±7.62	51.85±8.82	55.83±12.38	51.10±11.01	52.27±12.06	68.39±13.84
accident_volume_level	Chicago	43.09±11.96	42.77±12.15	46.90±13.71	43.15±12.55	46.26±13.34	48.83±13.68
	SF	55.85±11.48	58.07±10.67	58.31±10.86	58.40±10.61	58.43±11.10	58.10±11.37
	NY	37.14±10.59	35.72±10.21	39.22±13.34	35.86±12.14	36.01±13.09	50.17±14.79
risk_level	Chicago	34.19±7.29	34.02±7.68	40.49±12.05	33.90±9.30	37.74±11.12	43.95±12.63
	SF	39.47±11.15	40.98±10.84	41.26±11.59	41.76±12.48	41.41±11.76	42.34±12.20
	NY	41.46±11.21	42.06±11.21	47.30±13.63	41.40±12.38	42.80±13.05	57.24±14.23
Average	–	48.23	48.97	<u>52.50</u>	49.02	50.90	57.17

Table 2 summarizes three downstream tasks across three cities, yielding nine classification settings in total. FractalGCL attains the highest accuracy in eight of the nine settings and lifts the overall average to **57.17%**, an impressive **6.27%** lead over the next-best model, SimGRACE (50.90%). We attribute this gain to the strongly fractal nature of urban networks, which makes a fractal-aware approach especially effective; further details appear in Appendix B and publicly available code.

4.4 Ablation Study

Table 3: (a) Ablation study

Method	Components		MUTAG	
	Ren.	Frac. Loss	Acc.	Time (s)
FractalGCL	✓	✓	91.71	486.81
w/o. Graph Concat	✓	✓	90.41	321.87
w/o. Renormalisation	✗	✓	88.46	33.93
w/o. Fractal Loss	✓	✗	88.09	423.97
w/. Exact Dimension	✓	✓	90.32	1249.74

Table 4: (b) Variant accuracy

Variant	D&D	MUTAG
FractalGCL	80.14	91.71
+ random radius	78.78	88.73
+ R^2 prob.	79.80	88.83
– R^2 threshold	79.63	88.33

Table 3 lists MUTAG accuracy and pre-training time as we remove FractalGCL’s three key components—graph concatenation, renormalisation, and the fractal-dimension loss—one at a time. Dropping any single component lowers accuracy by about 1.3–3.6 pp, confirming that each part is essential. In terms of efficiency, our Gaussian surrogate for box-dimension estimation trims training time from 1249.74 s (w/. Exact Dimension) to 486.81 s, nearly a $2.56 \times$ speed-up—that is, roughly a 61 % reduction in compute.

4.5 Variant Experiments

Table 4 compares three ways of altering the renormalisation rule. Introducing a random radius or discarding the fractality filter both weaken the structural match between views and lower accuracy, while using R^2 merely as a soft sampling probability yields a middle-ground result. These variants confirm that a fixed small radius combined with an explicit R^2 threshold offers the best balance between view diversity and global consistency.

4.6 Parameter Analysis

Figure 6 shows that FractalGCL is robust to reasonable hyper-parameter changes: accuracy varies within about one percentage point across all tested settings. A moderate fractality filter ($R^2 \approx 0.9$) and a small dimension weight ($\alpha \leq 0.3$) already captures most of the gain, while larger penalties or very loose filters begin to erode performance. Batch size has little impact, confirming that the method scales smoothly without delicate tuning of training throughput.

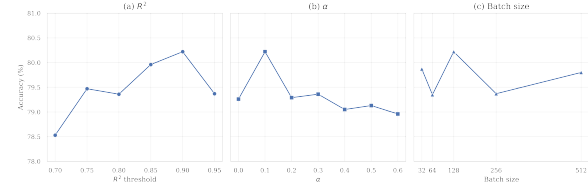


Figure 6: Hyper-parameter sensitivity on D&D

5 Related Works

Fractal Geometry for Graphs. Fractal geometry interfaces with graph theory most tangibly through the study of complex networks [37, 1, 32]. Analytical models of genuinely fractal graphs remain comparatively scarce. Recently, the Iterated Graph Systems framework has gained attention for its rigorous yet flexible recursive construction of fractal graphs [15, 26]. However, applications of fractal geometry within graph representation learning are still rare.

Graph Contrastive Learning. Graph contrastive learning comprises several crucial stages, among which graph data augmentation assumes a pivotal role, yet it is rendered particularly challenging by the intricate non-Euclidean characteristics inherent in graph topologies [13]. Existing graph data augmentation techniques [36, 46, 44, 28, 18, 38, 11, 10] have achieved notable progress. However, they often fall short in adequately preserving the structural similarity between positive pairs, which arises from the inherent difficulty in precisely leveraging complex topological features.

6 Conclusion

We present FractalGCL, a theoretically grounded graph-contrastive framework that couples renormalisation-based global views with a fractal-dimension-aware loss, unifying local perturbations and global topology. It achieves SOTA accuracy on four of six benchmarks and real-world networks; it also cuts training time nearly four times with a one-shot dimension estimator.

A limitation of FractalGCL is that, on the graphs that do not exhibit fractal structure, its empirical performance may lag behind the results obtained on datasets with pronounced fractal patterns. However, we believe that FractalGCL is not only a compelling demonstration of how fractal geometry can be integrated into machine learning, but also a foundational cornerstone for future research on fractal networks. We intend to continue investigating this line of research in future studies.

References

- [1] Albert-László Barabási and Réka Albert. Emergence of scaling in random networks. *science*, 286(5439):509–512, 1999.
- [2] Zefeng Chen, Wensheng Gan, Jiayang Wu, Kaixia Hu, and Hong Lin. Data scarcity in recommendation systems: A survey. *ACM Transactions on Recommender Systems*, 3(3):1–31, 2025.
- [3] Gerald A Edgar and Gerald A Edgar. *Measure, topology, and fractal geometry*, volume 2. Springer, 2008.
- [4] Kenneth Falconer. *Fractal geometry: mathematical foundations and applications*. John Wiley & Sons, 2013.
- [5] Mikhael Gromov, Misha Katz, Pierre Pansu, and Stephen Semmes. *Metric structures for Riemannian and non-Riemannian spaces*, volume 152. Springer, 1999.
- [6] R Devon Hjelm, Alex Fedorov, Samuel Lavoie-Marchildon, Karan Grewal, Phil Bachman, Adam Trischler, and Yoshua Bengio. Learning deep representations by mutual information estimation and maximization. *arXiv preprint arXiv:1808.06670*, 2018.
- [7] Weihua Hu, Bowen Liu, Joseph Gomes, Marinka Zitnik, Percy Liang, Vijay Pande, and Jure Leskovec. Strategies for pre-training graph neural networks. *arXiv preprint arXiv:1905.12265*, 2019.
- [8] Weihua Hu, Bowen Liu, Joseph Gomes, Marinka Zitnik, Percy Liang, Vijay Pande, and Jure Leskovec. Strategies for pre-training graph neural networks. In *International Conference on Learning Representations*, 2020.
- [9] Chao Huang, Xubin Ren, Jiabin Tang, Dawei Yin, and Nitesh Chawla. Large language models for graphs: Progresses and directions. In *Companion Proceedings of the ACM Web Conference 2024*, pages 1284–1287, 2024.

[10] Qirui Ji, Jiangmeng Li, Jie Hu, Rui Wang, Changwen Zheng, and Fanjiang Xu. Rethinking dimensional rationale in graph contrastive learning from causal perspective. In *Proceedings of the AAAI Conference on Artificial Intelligence*, volume 38, pages 12810–12820, 2024.

[11] Ming Jin, Yizhen Zheng, Yuan-Fang Li, Chen Gong, Chuan Zhou, and Shirui Pan. Multi-scale contrastive siamese networks for self-supervised graph representation learning. *arXiv preprint arXiv:2105.05682*, 2021.

[12] Wei Ju, Yiyang Gu, Xiao Luo, Yifan Wang, Haochen Yuan, Huasong Zhong, and Ming Zhang. Unsupervised graph-level representation learning with hierarchical contrasts. *Neural Networks*, 158:359–368, 2023.

[13] Wei Ju, Yifan Wang, Yifang Qin, Zhengyang Mao, Zhiping Xiao, Junyu Luo, Junwei Yang, Yiyang Gu, Dongjie Wang, Qingqing Long, et al. Towards graph contrastive learning: A survey and beyond. *arXiv preprint arXiv:2405.11868*, 2024.

[14] Thomas N Kipf and Max Welling. Variational graph auto-encoders. *arXiv preprint arXiv:1611.07308*, 2016.

[15] Nero Ziyu Li and Thomas Britz. On the scale-freeness of random colored substitution networks. *Proceedings of the American Mathematical Society*, 152(04):1377–1389, 2024.

[16] Ran Li, Shimin Di, Lei Chen, and Xiaofang Zhou. Gradgcl: Gradient graph contrastive learning. In *2024 IEEE 40th International Conference on Data Engineering (ICDE)*, pages 1171–1184. IEEE, 2024.

[17] Sihang Li, Xiang Wang, An Zhang, Yingxin Wu, Xiangnan He, and Tat-Seng Chua. Let invariant rationale discovery inspire graph contrastive learning. In *International conference on machine learning*, pages 13052–13065. PMLR, 2022.

[18] Sihang Li, Xiang Wang, An Zhang, Yingxin Wu, Xiangnan He, and Tat-Seng Chua. Let invariant rationale discovery inspire graph contrastive learning. In *International conference on machine learning*, pages 13052–13065. PMLR, 2022.

[19] Jiawei Liu, Cheng Yang, Zhiyuan Lu, Junze Chen, Yibo Li, Mengmei Zhang, Ting Bai, Yuan Fang, Lichao Sun, Philip S Yu, et al. Towards graph foundation models: A survey and beyond. *arXiv preprint arXiv:2310.11829*, 2023.

[20] Yixin Liu, Ming Jin, Shirui Pan, Chuan Zhou, Yu Zheng, Feng Xia, and Philip S Yu. Graph self-supervised learning: A survey. *IEEE transactions on knowledge and data engineering*, 35(6):5879–5900, 2022.

[21] Yixin Liu, Yu Zheng, Daokun Zhang, Hongxu Chen, Hao Peng, and Shirui Pan. Towards unsupervised deep graph structure learning. In *Proceedings of the ACM Web Conference 2022*, pages 1392–1403, 2022.

[22] Benoit B Mandelbrot. The fractal geometry of nature/revised and enlarged edition. *New York*, 1983.

[23] Benoit B Mandelbrot. Fractal geometry: what is it, and what does it do? *Proceedings of the Royal Society of London. A. Mathematical and Physical Sciences*, 423(1864):3–16, 1989.

[24] Christopher Morris, Nils M Kriege, Franka Bause, Kristian Kersting, Petra Mutzel, and Marion Neumann. Tudataset: A collection of benchmark datasets for learning with graphs. *arXiv preprint arXiv:2007.08663*, 2020.

[25] Annamalai Narayanan, Mahinthan Chandramohan, Rajasekar Venkatesan, Lihui Chen, Yang Liu, and Shantanu Jaiswal. graph2vec: Learning distributed representations of graphs. *arXiv preprint arXiv:1707.05005*, 2017.

[26] Ziyu Neroli. Fractal dimensions for iterated graph systems. *Proceedings of the Royal Society A*, 480(2300):20240406, 2024.

[27] Chanyoung Park, Donghyun Kim, Jiawei Han, and Hwanjo Yu. Unsupervised attributed multiplex network embedding. In *Proceedings of the AAAI conference on artificial intelligence*, volume 34, pages 5371–5378, 2020.

[28] Jiezhong Qiu, Qibin Chen, Yuxiao Dong, Jing Zhang, Hongxia Yang, Ming Ding, Kuansan Wang, and Jie Tang. Gcc: Graph contrastive coding for graph neural network pre-training. In *Proceedings of the 26th ACM SIGKDD international conference on knowledge discovery & data mining*, pages 1150–1160, 2020.

[29] Yuxiang Ren, Jiyang Bai, and Jiawei Zhang. Label contrastive coding based graph neural network for graph classification. In *Database Systems for Advanced Applications: 26th International Conference, DASFAA 2021, Taipei, Taiwan, April 11–14, 2021, Proceedings, Part I* 26, pages 123–140. Springer, 2021.

[30] Yu Rong, Wenbing Huang, Tingyang Xu, and Junzhou Huang. Dropedge: Towards deep graph convolutional networks on node classification. *arXiv preprint arXiv:1907.10903*, 2019.

[31] Bo-Shen Shi, Yong-Qing Wang, Fang-Da Guo, Bing-Bing Xu, Hua-Wei Shen, and Xue-Qi Cheng. Domain adaptation for graph representation learning: Challenges, progress, and prospects. *Journal of Computer Science and Technology*, pages 1–18, 2025.

[32] Chaoming Song, Shlomo Havlin, and Hernan A Makse. Self-similarity of complex networks. *Nature*, 433(7024):392–395, 2005.

[33] Fan-Yun Sun, Jordan Hoffmann, Vikas Verma, and Jian Tang. Infograph: Unsupervised and semi-supervised graph-level representation learning via mutual information maximization. *arXiv preprint arXiv:1908.01000*, 2019.

[34] Mengying Sun, Jing Xing, Huijun Wang, Bin Chen, and Jiayu Zhou. Mocl: data-driven molecular fingerprint via knowledge-aware contrastive learning from molecular graph. In *Proceedings of the 27th ACM SIGKDD conference on knowledge discovery & data mining*, pages 3585–3594, 2021.

[35] Petar Velickovic, William Fedus, William L Hamilton, Pietro Liò, Yoshua Bengio, and R Devon Hjelm. Deep graph infomax. *ICLR (poster)*, 2(3):4, 2019.

[36] Petar Velickovic, William Fedus, William L Hamilton, Pietro Liò, Yoshua Bengio, and R Devon Hjelm. Deep graph infomax. *ICLR (poster)*, 2(3):4, 2019.

[37] Duncan J Watts and Steven H Strogatz. Collective dynamics of ‘small-world’ networks. *nature*, 393(6684):440–442, 1998.

[38] Chunyu Wei, Yu Wang, Bing Bai, Kai Ni, David Brady, and Lu Fang. Boosting graph contrastive learning via graph contrastive saliency. In *International conference on machine learning*, pages 36839–36855. PMLR, 2023.

[39] Lirong Wu, Haitao Lin, Cheng Tan, Zhangyang Gao, and Stan Z Li. Self-supervised learning on graphs: Contrastive, generative, or predictive. *IEEE Transactions on Knowledge and Data Engineering*, 35(4):4216–4235, 2021.

[40] Jun Xia, Lirong Wu, Jintao Chen, Bozhen Hu, and Stan Z Li. Simgrace: A simple framework for graph contrastive learning without data augmentation. In *Proceedings of the ACM web conference 2022*, pages 1070–1079, 2022.

[41] Jun Xia, Lirong Wu, Ge Wang, Jintao Chen, and Stan Z Li. Progcl: Rethinking hard negative mining in graph contrastive learning. In *International Conference on Machine Learning*, pages 24332–24346. PMLR, 2022.

[42] Yaochen Xie, Zhao Xu, Jingtun Zhang, Zhengyang Wang, and Shuiwang Ji. Self-supervised learning of graph neural networks: A unified review. *IEEE transactions on pattern analysis and machine intelligence*, 45(2):2412–2429, 2022.

[43] Keyulu Xu, Weihua Hu, Jure Leskovec, and Stefanie Jegelka. How powerful are graph neural networks? *arXiv preprint arXiv:1810.00826*, 2018.

- [44] Yuning You, Tianlong Chen, Yang Shen, and Zhangyang Wang. Graph contrastive learning automated. In *International conference on machine learning*, pages 12121–12132. PMLR, 2021.
- [45] Yuning You, Tianlong Chen, Yang Shen, and Zhangyang Wang. Graph contrastive learning automated. In *International conference on machine learning*, pages 12121–12132. PMLR, 2021.
- [46] Yuning You, Tianlong Chen, Yongduo Sui, Ting Chen, Zhangyang Wang, and Yang Shen. Graph contrastive learning with augmentations. *Advances in neural information processing systems*, 33:5812–5823, 2020.
- [47] Xuehao Zhai, Junqi Jiang, Adam Dejl, Antonio Rago, Fangce Guo, Francesca Toni, and Aruna Sivakumar. Heterogeneous graph neural networks with post-hoc explanations for multi-modal and explainable land use inference. *Information Fusion*, 120:103057, 2025.
- [48] Hengrui Zhang, Qitian Wu, Yu Wang, Shaofeng Zhang, Junchi Yan, and Philip S Yu. Localized contrastive learning on graphs. *arXiv preprint arXiv:2212.04604*, 2022.
- [49] Jiahui Zhao, Pan Liu, and Zhibin Li. Exploring the impact of trip patterns on spatially aggregated crashes using floating vehicle trajectory data and graph convolutional networks. *Accident Analysis & Prevention*, 194:107340, 2024.

Appendix

A Proofs

A rigorous mathematical approach to define and analyse “fractal graphs” relies on viewing a graph as a metric space and studying its *scaling limit* in the sense of Gromov-Hausdorff topology. Concretely, in this section, let $G = (V, E)$ be a simple, connected infinite graph with its shortest-path metric. A sequence of such graphs (\hat{G}^n) is said to converge to a limiting metric space \hat{G}^∞ if

$$\lim_{n \rightarrow \infty} d_{\text{GH}}(\hat{G}^n, \hat{G}^\infty) = 0,$$

where d_{GH} is the Gromov–Hausdorff distance. If the limit \hat{G}^∞ exhibits fractal behaviour, then the original sequence (G^n) is often viewed to possess fractality in a limiting sense.

Although this framework is theoretically well-founded and widely studied in the context of metric geometry and fractal analysis, it typically introduces extensive technical details. In real-world problems involving large-scale networks (e.g., deep neural architectures, biological networks, or social graphs), a full treatment of Gromov–Hausdorff convergence can be unnecessarily complex. Consequently, the present work uses the notion of “infinite graphs” and “fractal-like structures” primarily as an intuitive and useful abstraction of multi-scale patterns, rather than relying on a strict Gromov–Hausdorff scaling limit argument. Readers interested in the detailed mathematical background are referred to [4, 5, 26] for further discussion.

Definition A.1 (Definition 3.1). *Let G be an (infinite) graph equipped with a graph distance d_G . An L box-covering of G is a collection of subgraphs $\{U_i\}_{i \in \mathcal{I}}$ where \mathcal{I} is an index set, such that:*

$$\bigcup_{i \in \mathcal{I}} U_i = G \quad \text{and} \quad \text{diam}(U_i) \leq L \quad \forall i \in \mathcal{I}.$$

Here, $\text{diam}(U_i)$ refers to the diameter of U_i regarding metric d_G . We denote by $N_L(G)$ the minimum number of subgraphs needed for an L box-covering of G . Then the Minkowski dimension (also called the box dimension) of G is given by

$$\dim_B(G) := \lim_{L/\text{diam}(G) \rightarrow 0} \frac{\log N_L(G)}{-\log \frac{L}{\text{diam}(G)}},$$

provided this limit exists.

If $\dim_B(G)$ is both finite and strictly positive, we say that G possesses a fractal property, and we refer to G as a Minkowski graph.

Algorithm 1 Algorithm of computing box dimension

Let G be a finite graph. Denote by d the diameter of G , i.e., the maximum shortest-path length between any two nodes. If $d \leq 9$, the scale is considered too small for fractal analysis and the algorithm terminates without output.

For a scale parameter $l \in \{1, 2, \dots, L_{\max}\}$, with $L_{\max} = \lfloor d/2 \rfloor$, define the covering radius as $r = \lfloor l/2 \rfloor$. At each scale l , a greedy box-covering algorithm is applied to compute the number of boxes $N_B(l)$ needed to cover G :

- **Even l :** Let U be the set of uncovered nodes. Repeatedly, select a node $v \in U$ whose ball $B(v, r)$ (i.e., the set of nodes within distance r from v) covers the maximum number of nodes in U . Remove $B(v, r)$ from U and count one box. Continue until U is empty.
- **Odd l :** First, attempt to select a pair of adjacent nodes (v, w) from U as dual centres. Define the covering set as $B(v, r) \cup B(w, r)$. If such a pair exists that maximizes the coverage of U , remove the union from U and count one box. If no suitable pair is found, revert to the single-centre method as in the even case.

Thus, for each l , one obtains a data point $(l, N_B(l))$. Assuming that the box-covering number obeys a power-law relation $N_B(l) \sim l^{-\dim_B(G)}$, where $\dim_B(G)$ is the box (fractal) dimension, taking logarithms yields $\log N_B(l) = -\dim_B(G) \log l + b$. By performing a least-squares linear regression on the data points $\{(\log l, \log N_B(l))\}$, we fit the model $y = mx + b$, and define the fractal dimension as

$$\dim_B(G) = -m.$$

The coefficient of determination, R^2 , quantifies the goodness-of-fit of the log-log linear model; values of R^2 close to 1 indicate a strong power-law (self-similar) behaviour of the graph. The algorithm outputs the pair $(R^2, \dim_B(G))$ as the evaluation result of the graph's fractal properties.

Algorithm 2 Three-Step Random-Centre Renormalisation

Input. Graph G with adjacency A , radius r . **Output.** Renormalised graph $\mathcal{R}(G)$.

1. **Random centre selection.** While vertices remain, uniformly pick a centre u , and form a super node $U = \{v \mid (\sum_{i=1}^r A^i)_{uv} > 0\} \cup \{u\}$; delete U from the pool.
2. **Assignment matrix.** Record all super nodes in a binary matrix S with $s_{ij} = 1$ iff vertex j belongs to super node i .
3. **Graph reconstruction.** Compute $A_{\text{super}} = SAS^\top$ and define $\mathcal{R}(G)$ on this adjacency.

Theorem A.2 (Theorem 3.3).

$$\dim_B(\mathcal{R}(G)) = \dim_B(G).$$

Proof. Denote by $N_L(G)$ the minimum number of L -box-covering sets of G , and let $N_L(\mathcal{R}(G))$ be the analogous quantity for the renormalised graph.

Any L -covering of G naturally induces an L -covering of $\mathcal{R}(G)$. Indeed, since each “supervertex” in $\mathcal{R}(G)$ corresponds to one of the L -boxes in G , you can treat each box as if it were “collapsed” into a single node. Therefore,

$$N_L(\mathcal{R}(G)) \leq N_L(G).$$

Conversely, given an L -covering of $\mathcal{R}(G)$, one can “expand” each supervertex v_i back to the corresponding box U_i in G . Since edges between two supervertices in $\mathcal{R}(G)$ indicate there was a connection between the respective U_i and U_j in G , the covering in $\mathcal{R}(G)$ lifts to an L' -covering of G (where L' is of the same order as L , up to a possible constant factor). Hence we obtain a bound of the form

$$N_L(G) \leq c N_L(\mathcal{R}(G)),$$

for some absolute constant c .

Combining these bounds yields $c N_L(G) \leq N_L(\mathcal{R}(G)) \leq N_L(G)$, where c is a positive constant independent of L . Finally,

$$\begin{aligned} \dim_B(G) &= \lim_{L/\text{diam}(G) \rightarrow 0} \frac{\log(cN_L(G))}{-\log \frac{L}{\text{diam}(G)}} \\ &\leq \lim_{L/\text{diam}(G) \rightarrow 0} \frac{\log(N_L(G) + \log c)}{-\log \frac{L}{\text{diam}(G)}} \\ &\leq \dim_B(\mathcal{R}(G)) \leq \dim_B(G). \end{aligned}$$

□

Proposition A.3 (Dimension–Dominated Ranking Consistency). *If $\Delta_1 < \Delta_2$ and $s_1 - s_2 \leq \varepsilon$, for $\varepsilon := \tau \alpha(\Delta_2 - \Delta_1)$, then the fractal-weighted InfoNCE losses satisfy*

$$\ell_{\text{fractal}}(G, H_2) < \ell_{\text{fractal}}(G, H_1).$$

Proof. For each candidate H_i , the single-sample fractal loss is

$$\ell_{\text{fractal}}(G, H_i) = -\frac{s_i}{\tau} - \log w_i + \log Z, \quad i = 1, 2,$$

where Z is the common partition term. Taking the difference,

$$\ell_{\text{fractal}}(G, H_2) - \ell_{\text{fractal}}(G, H_1) = -\frac{s_2 - s_1}{\tau} - \log \frac{w_2}{w_1}.$$

Since $\Delta_2 > \Delta_1$ and $w_i = \exp(\alpha\Delta_i)$, we have

$$\log \frac{w_2}{w_1} = \alpha(\Delta_2 - \Delta_1) > 0.$$

By the assumption $s_1 - s_2 \leq \varepsilon = \tau\alpha(\Delta_2 - \Delta_1)$, it follows that

$$-\frac{s_2 - s_1}{\tau} \leq \alpha(\Delta_2 - \Delta_1),$$

hence the difference of losses is negative:

$$\ell_{\text{fractal}}(G, H_2) - \ell_{\text{fractal}}(G, H_1) < 0.$$

Therefore $\ell_{\text{fractal}}(G, H_2) < \ell_{\text{fractal}}(G, H_1)$, completing the proof. □

Proposition A.4 (Fractal complexity on sparse graphs). *For the greedy box-covering procedure in Algorithm 3, applied to any connected sparse graph with V vertices, the worst-case running time $T(V)$ obeys*

$$\Omega(V^2) \leq T(V) \leq O(V^3).$$

Proof. Lower bound $\Omega(V^2)$. Consider a path of V vertices. At the smallest scale (covering radius 1) a single box covers at most two vertices, so roughly $V/2$ boxes must be chosen. Each choice is made by scanning *all* currently uncovered vertices to find the one whose radius-1 neighbourhood is largest: first V scans, then $V-1$, and so on. The total number of vertex inspections is $V + (V-1) + \dots + 1 = \Theta(V^2)$, establishing a $\Omega(V^2)$ lower bound for this single scale; hence $T(V) \geq \Omega(V^2)$.

Upper bound $O(V^3)$. The algorithm repeats this greedy covering for every scale $l = 1, \dots, \lfloor V/2 \rfloor$, that is, at most $O(V)$ distinct scales. For any fixed scale, at most V boxes are chosen. In a sparse graph, computing the radius- $l/2$ neighbourhood of a vertex via BFS touches $O(V)$ edges, so one scale costs $O(V) \times O(V) = O(V^2)$ time. Multiplying by $O(V)$ scales gives the global upper bound $T(V) = O(V^3)$.

Thus the worst-case complexity satisfies $\Omega(V^2) \leq T(V) \leq O(V^3)$. □

Lemma A.5. *For a graph G with diameter $\text{diam}(G)$, the standard error of linear regression for the Minkowski dimension satisfies*

$$SE(\hat{m}) \sim \sqrt{6}\sigma \frac{1}{\sqrt{\text{diam}(G) \log \text{diam}(G)}}.$$

Proof. For a uniform distribution on the interval $[0, \log(\lfloor \text{diam}(G)/2 \rfloor)]$, the variance is given by

$$\text{Var}(x) = \frac{(\log(\lfloor \text{diam}(G)/2 \rfloor))^2}{12}.$$

If there are $n = \lfloor \text{diam}(G)/2 \rfloor$ data points, then the total sum of squares about the mean is

$$S_{xx} = \lfloor \text{diam}(G)/2 \rfloor \cdot \frac{(\log(\lfloor \text{diam}(G)/2 \rfloor))^2}{12}.$$

Let σ be the residual standard deviation. We obtain

$$\text{SE}(\hat{m}) = \sigma \sqrt{\frac{12}{\lfloor \text{diam}(G)/2 \rfloor (\log(\lfloor \text{diam}(G)/2 \rfloor))^2}}$$

As a result,

$$\lim_{n \rightarrow \infty} \frac{\text{SE}(\hat{m})}{(\sqrt{\text{diam}(G)} \log \text{diam}(G))^{-1}} = \lim_{n \rightarrow \infty} \frac{\sqrt{12}\sigma}{\sqrt{2}} \frac{1}{\sqrt{\text{diam}(G)}(\log \text{diam}(G) - \log 2)} = \sqrt{6}\sigma$$

This completes the proof. \square

Hypothesis A.6. *1. **Residuals.** For each scale l , the log-regression errors ε_l (on G) and $\varepsilon_l^{\mathcal{R}}$ (on $\mathcal{R}(G)$) are independent, centred, and share the same finite variance σ^2 and finite fourth moment.*

2. **Design matrix growth.** With $x_i = \log(1/r_i)$ and $n = \lfloor \text{diam}(G)/2 \rfloor$, we have $\frac{1}{n} \sum_{i=1}^n x_i = 0$ and $\frac{1}{n} \sum_{i=1}^n x_i^2 \rightarrow \mathbb{E}[X^2]$ as $n \sim \text{diam}(G)/2 \rightarrow \infty$.
3. **Cross-graph independence.** The two residual sequences $\{\varepsilon_l\}_l$ and $\{\varepsilon_l^{\mathcal{R}}\}_l$ are mutually independent (or weakly dependent in a way that preserves the OLS CLT).
4. **True-slope convergence.** The box dimension of the renormalised infinite graph equals that of the original graph, implying $m_{\mathcal{R}} - m_G \rightarrow 0$ as $\text{diam}(G) \rightarrow \infty$ (cf. Theorem 3.3).

Theorem A.7 (Gaussian limit of $\Delta(G)$). *Let μ_G be the probability measure induced by the random variable $\Delta(G) = \dim(G) - \dim(\mathcal{R}(G))$ on a graph G of diameter $D = \text{diam}(G)$. Under Hypothesis A.6 and with the notation of Lemmas 3.7–3.8, we have*

$$\mu_G \xrightarrow{w} \mathcal{N}(0, \tau^2(D)), \quad \tau^2(D) = 6\sigma^2 [D(\log D)^2]^{-1},$$

as $D \rightarrow \infty$. In particular, $\tau^2(D) \rightarrow 0$, so the limiting distribution degenerates to the Dirac measure δ_0 ; i.e. $\Delta(G) \rightarrow 0$ in probability.

Proof. Recall that the box dimension of a finite graph is estimated by the negative OLS slope \hat{m} obtained from the log–log regression $\log N_B(l) = m \log l + b + \varepsilon_l$. Denote the corresponding true slopes of G and $\mathcal{R}(G)$ by m_G and $m_{\mathcal{R}}$, and their estimators by $\hat{m}_G, \hat{m}_{\mathcal{R}}$. By definition

$$\Delta(G) = \hat{m}_G - \hat{m}_{\mathcal{R}} + (m_{\mathcal{R}} - m_G). \quad (5)$$

Step 1: asymptotic distribution of the two slope estimators. Under Assumptions (A1)–(A3) of Hypothesis A.6 and by Lemma 3.8,

$$\sqrt{D}(\hat{m}_G - m_G) \xrightarrow{d} \mathcal{N}(0, \sigma^2), \quad \sqrt{D}(\hat{m}_{\mathcal{R}} - m_{\mathcal{R}}) \xrightarrow{d} \mathcal{N}(0, \sigma^2),$$

while the two limits are asymptotically independent thanks to the cross-graph independence in (A3).

Step 2: variance of their difference. Subtracting the two Gaussian limits and dividing by \sqrt{D} gives

$$\sqrt{D}[(\hat{m}_G - m_G) - (\hat{m}_{\mathcal{R}} - m_{\mathcal{R}})] \xrightarrow{d} \mathcal{N}(0, 2\sigma^2).$$

Multiplying and dividing by the common factor $S_{xx}^{-1}(G) \sim 6/[D(\log D)^2]$ from Lemma 3.7, and noting that $S_{xx}(G) \sim S_{xx}(\mathcal{R}(G))$, we obtain the variance term in the statement,

$$\tau^2(D) = \frac{\sigma^2}{S_{xx}(G)} + \frac{\sigma^2}{S_{xx}(\mathcal{R}(G))} = 6\sigma^2 [D(\log D)^2]^{-1}.$$

Step 3: applying Slutsky's theorem. Assumption (A4) together with Theorem 3.3 implies $m_{\mathcal{R}} - m_G \rightarrow 0$ as $D \rightarrow \infty$. In (5) this term is therefore negligible relative to the $D^{-1/2}$ -scaled Gaussian component. Slutsky's theorem hence yields the weak convergence

$$\mu_G \xrightarrow{w} \mathcal{N}(0, \tau^2(D)), \quad \tau^2(D) = 6\sigma^2 [D(\log D)^2]^{-1}.$$

Step 4: degeneration to a Dirac measure. Because $\tau^2(D) \rightarrow 0$ as $D \rightarrow \infty$, the normal limit collapses to the Dirac measure δ_0 , which implies $\Delta(G) \rightarrow 0$ in probability; equivalently, $\mu_G \xrightarrow{w} \delta_0$. \square

Remark A.8. The phrase “with probability 1” in Theorem A.7 should be understood in the asymptotic sense $\text{diam}(G) \rightarrow \infty$. More precisely,

$$\Delta(G) \xrightarrow{p} 0 \iff \mathbf{P}(|\Delta(G)| > \varepsilon) \rightarrow 0 \quad (\forall \varepsilon > 0),$$

so the dimension discrepancy vanishes in probability. Equivalently, because the Gaussian law $\mathcal{N}(0, \tau^2(D))$ has variance $\tau^2(D) \rightarrow 0$, its distribution $\mu_{\Delta(G)}$ weakly converges to the Dirac measure δ_0 :

$$\lim_{\text{diam}(G) \rightarrow \infty} \int_{\mathbb{R}} \phi(x) d\mu_{\Delta(G)}(x) = \phi(0) \quad \text{for every bounded continuous } \phi.$$

Hence, in the infinite-scale limit the fractal dimensions of G and $\mathcal{R}(G)$ become statistically indistinguishable.

Remark A.9. The main theorem shows that, with uniform log-scale sampling and i.i.d. Gaussian residuals, the gap $\Delta(G) = \text{dim}(G) - \text{dim}(\mathcal{R}(G))$ is asymptotically normal, $\Delta(G) \sim \mathcal{N}(0, \tau^2(D))$ with

$$\tau^2(\text{diam}(G)) = \frac{6\hat{\sigma}^2}{\text{diam}(G) [\log \text{diam}(G)]^2} \rightarrow 0$$

so the two dimensions become statistically indistinguishable as $D \rightarrow \infty$.

B Detailed Preliminary Experimental Results

B.1 Preliminary Experiments

Preliminary Experiment 1 We assessed the prevalence of fractal structure across six TU datasets by applying Algorithm 1 (Appendix A) to every graph. For each graph, we fitted a box-counting regression and recorded its coefficient of determination R^2 ; the counts and percentages above four thresholds are summarised in Table 5. The statistics show that strongly fractal graphs ($R^2 \geq 0.90$) dominate most datasets, supporting the motivation for fractal-based augmentations used in the main paper.

Table 5: Number (%) of graphs whose box-counting R^2 exceeds each threshold.

Dataset	$R^2 > 0.50$	$R^2 > 0.80$	$R^2 > 0.90$	$R^2 > 0.95$
PROTEINS (1 113)	979 (87.96%)	968 (86.97%)	905 (81.31%)	711 (63.88%)
MUTAG (188)	188 (100.00%)	172 (91.49%)	136 (72.34%)	74 (39.36%)
NCII (4 110)	4 108 (99.95%)	3 979 (96.81%)	3 277 (79.73%)	1 817 (44.21%)
D&D (1 178)	1 178 (100.00%)	1 178 (100.00%)	1 176 (99.83%)	1 155 (98.05%)
REDDIT-B (2 000)	1 971 (98.55%)	1 875 (93.75%)	1 419 (70.95%)	577 (28.85%)
REDDIT-M5K (4 999)	4 999 (100.00%)	4 985 (99.72%)	4 599 (92.00%)	2 215 (44.31%)

Preliminary Experiment 2 This pilot study quantifies how much predictive power the **box dimension** adds when only a handful of cheap, global graph statistics are available. We follow a controlled 10-fold cross-validation protocol with the steps and rationale detailed below.

- Data loading and preprocessing.** Six TU datasets are read from the pre-computed CSV files in `R2_num_data/*.csv`, each row containing `graph_id`, `label1`, and several graph-level attributes such as `degree_variance`, `avg_shortest_path`, and `box_dimension`. All features are fed to the classifier as raw values; no scaling is required for random forests, though a `StandardScaler` could be inserted if a linear model were used later.

2. Feature sets.

- *Baseline*: $\{\text{degree_variance}, \text{avg_shortest_path}\}$.
- *Baseline + BoxDim*: baseline features plus `box_dimension`.

Keeping all else equal isolates the incremental contribution of the box dimension.

3. Classifier and cross-validation.

- **Model:** `RandomForestClassifier` (200 trees, default hyper-parameters, `random_state=42, n_jobs=-1`). Random forests are robust to feature scales, nearly saturated with such a small feature set, and easy to interpret.
- **Evaluation:** stratified 10-fold CV (`shuffle=True, random_state=42`) to preserve class balance.
- 4. **Paired statistical test.** Each dataset yields two 10-element accuracy vectors, $\{\text{Acc}_{\text{base},k}\}_{k=1}^{10}$ and $\{\text{Acc}_{\text{full},k}\}_{k=1}^{10}$. A two-tailed **paired *t*-test** is applied to their differences $d_k = \text{Acc}_{\text{full},k} - \text{Acc}_{\text{base},k}$. A *p*-value under 0.05 indicates that adding the box dimension yields a statistically significant improvement under the same train/test splits.
- 5. **Result recording.** For each dataset we log (i) mean \pm std of baseline and augmented accuracies, (ii) mean ΔAcc , and (iii) the paired *p*-value. All numbers are written to `boxdim_incremental_results_6datasets.csv`, ready for direct L^AT_EX table conversion via `DataFrame.to_latex`.

This rigorous design keeps the *only* independent variable—whether the box dimension is present—under control, allowing us to test the hypothesis that *the box dimension provides significant additional discriminative information over traditional global graph statistics*. See Table 6 for full results.

Table 6: Incremental effect of adding `box_dimension`. Accuracies are given in percentage points (%) with one-standard-deviation error; ΔAcc is the mean paired gain in points and *p*-values come from a two-tailed paired *t*-test.

Dataset	Accuracy \pm std (%)		ΔAcc (%)	<i>p</i> -value
	Baseline	+BoxDim		
PROTEINS	67.75 ± 3.63	69.90 ± 3.39	+2.15	9.30×10^{-2}
MUTAG	83.54 ± 5.92	85.64 ± 6.67	+2.11	2.70×10^{-1}
NCII	62.51 ± 2.16	64.67 ± 1.51	+2.17	2.23×10^{-2}
D&D	67.15 ± 3.30	71.64 ± 2.58	+4.50	9.72×10^{-4}
REDDIT-BINARY	79.25 ± 2.94	80.80 ± 2.12	+1.55	4.13×10^{-2}
REDDIT-MULTI-5K	33.33 ± 1.58	38.19 ± 1.71	+4.86	2.25×10^{-4}

C Experimental Methodology and Results of FractalGCL on Urban Districts

In this section we present the overall experimental framework for evaluating the performance of FractalGCL embeddings on urban districts in three major cities (Chicago, San Francisco and New York).

C.1 Setup

Our pipeline consists of three complementary data modalities extracted for each equal-area “catchment”:

- **Road Subgraph Structure:** From the full city road network, we clip each catchment’s local subgraph of nodes and edges, preserving the topological patterns characteristic of that district.
- **Static Spatial Features:** We compute population density and six categories of point-of-interest densities (office, sustenance, transportation, retail, leisure and residence), thereby capturing the functional profile of each catchment.

- **Accident Statistics:** Drawing on historical crash data, we aggregate total accident counts and severity level breakdowns to assess safety-risk characteristics of each catchment.

The high-level experimental logic proceeds as follows:

1. Graph Embedding Generation.

- *FractalGCL Contrastive Training:* We train FractalGCL on the set of catchment subgraphs to produce fixed-dimensional node and graph embeddings that respect both topology and feature distributions.
- *Baseline Encoders:* In parallel, we train several established graph contrastive methods (e.g. DGI, InfoGraph, SimGRACE) to serve as performance benchmarks.

2. Multi-Task Classification Evaluation.

- *Accident-Related Tasks:* We formulate a suite of binary, multi-class and ordinal classification tasks based on accident counts and severity distributions (e.g. high vs. low total accidents, severity entropy, risk levels).
- *Functional Feature Tasks:* We also define multi-class tasks over the static POI and density features (e.g. dominant land-use category, mixture entropy level, population density tier, function-density combinations).

3. Performance Comparison and Analysis.

- For each task, we extract embeddings from each encoder and train a (linear) SVM under repeated stratified cross-validation.
- We compare accuracy and stability metrics across all encoders to quantify the advantages of FractalGCL in integrating topological, functional, and safety information.

C.2 Hyperparameter Configuration

In all experiments across Chicago, San Francisco and New York, we used a single, fixed set of hyperparameters for both FractalGCL and the baseline encoders. Specifically, each mini-batch consisted of 16 graph-level instances, and our GraphSAGE backbone employed two convolutional layers with 64 hidden channels apiece. The final projection head produced 128-dimensional embeddings for each graph. For contrastive augmentations we applied edge dropping with probability 0.1, and in FractalGCL we injected fractal noise weighted by $\alpha = 0.4$ after a renormalisation step with radius $r = 1.0$. All models were trained for 20 epochs using the Adam optimizer with a learning rate of 10^{-3} . These settings were held constant to ensure that any observed performance differences arose solely from the encoding method itself rather than hyperparameter variations.

C.3 Traffic Accident Classification Tasks

We evaluate each embedding method on six downstream classification tasks based on catchment accident statistics. Below we list each task name and its precise definition:

total_accidents_high

Binary classification: label = 1 if total accident count \geq city median, else 0. Tests the ability to separate high-accident vs. low-accident districts.

accident_volume_level

Three-class classification: split total accidents into Low/Medium/High tiers by the 33% and 67% quantiles, labeled 0/1/2. Assesses gradated accident volume encoding.

severity_entropy

Binary classification: compute Shannon entropy of severity-level proportions $\{p_i\}_{i=1}^4$, then label = 1 if entropy $>$ median, else 0. Measures embedding of severity diversity.

has_sev3 and has_sev4

Binary classification:

- *has_sev3:* label = 1 if at least one Severity-3 accident occurred, else 0.
- *has_sev4:* label = 1 if at least one Severity-4 accident occurred, else 0.

Evaluates detection of any serious crashes independently of total counts.

`risk_level`

Three-class ordinal classification: combine accident volume and severe-accident ratio:

$$\text{label} = \begin{cases} 2 & \text{if volume} > \text{median and } (\text{sev3} + \text{sev4})/\text{total} > \text{median,} \\ 0 & \text{if volume} \leq \text{median and } (\text{sev3} + \text{sev4})/\text{total} \leq \text{median,} \\ 1 & \text{otherwise.} \end{cases}$$

Captures joint severity–volume risk levels.

For each task, we extract graph-level embeddings from each encoder and perform repeated stratified 10-fold cross-validation using a linear SVM. Reported metrics are mean accuracy \pm standard deviation over 1000 repeats.

Please find full results in Table 7.

Table 7: Performance (mean \pm std) on traffic-safety tasks; numbers are in percentage points.

Task	City	DGI	InfoGraph	GCL	JOAO	SimGRACE	FractalGCL
total.accidents.high	Chicago	54.91 \pm 10.75	56.54 \pm 11.85	63.12 \pm 13.36	55.86 \pm 12.21	62.75 \pm 13.50	64.60\pm13.32
	SF	76.45 \pm 14.47	78.74 \pm 13.60	80.06 \pm 13.32	79.75 \pm 13.61	80.40 \pm 13.47	80.89\pm12.92
	NY	51.51 \pm 7.62	51.85 \pm 8.82	55.83 \pm 12.38	51.10 \pm 11.01	52.27 \pm 12.06	68.39\pm13.84
accident_volume_level	Chicago	43.09 \pm 11.96	42.77 \pm 12.15	46.90 \pm 13.71	43.15 \pm 12.55	46.26 \pm 13.34	48.83\pm13.68
	SF	55.85 \pm 11.48	58.07 \pm 10.67	58.31 \pm 10.86	58.40 \pm 10.61	58.43\pm11.10	58.10 \pm 11.37
	NY	37.14 \pm 10.59	35.72 \pm 10.21	39.22 \pm 13.34	35.86 \pm 12.14	36.01 \pm 13.09	50.17\pm14.79
severity_entropy	Chicago	50.99 \pm 7.10	52.64 \pm 9.11	58.87 \pm 12.33	52.38 \pm 9.60	57.07 \pm 11.97	65.60\pm13.22
	SF	49.04 \pm 4.75	49.03 \pm 6.39	48.86 \pm 9.93	48.98 \pm 11.00	48.96 \pm 9.93	49.15\pm10.60
	NY	52.23 \pm 8.21	51.86 \pm 8.61	54.45 \pm 11.82	51.63 \pm 11.03	52.40 \pm 12.00	61.27\pm13.49
has_sev3	Chicago	80.09 \pm 18.52	79.25 \pm 17.82	80.82\pm14.07	79.65 \pm 16.10	80.79 \pm 14.96	80.48 \pm 14.16
	SF	98.04\pm0.31	97.50 \pm 6.45	97.81 \pm 3.73	97.11 \pm 4.27	97.82 \pm 3.62	97.66 \pm 3.84
	NY	55.68 \pm 14.73	55.96 \pm 14.92	57.37 \pm 14.83	54.69 \pm 15.12	55.75 \pm 15.25	64.82\pm13.53
has_sev4	Chicago	53.90 \pm 10.67	54.00 \pm 10.17	60.37 \pm 13.48	54.02 \pm 11.12	59.76 \pm 13.76	62.74\pm13.66
	SF	54.73 \pm 13.45	53.91 \pm 14.23	55.50 \pm 13.15	54.95 \pm 13.75	55.40 \pm 13.71	56.44\pm14.51
	NY	52.44 \pm 11.64	53.33 \pm 12.15	56.22 \pm 13.55	53.34 \pm 13.71	54.89 \pm 14.07	59.88\pm13.23
risk_level	Chicago	34.19 \pm 7.29	34.02 \pm 7.68	40.49 \pm 12.05	33.90 \pm 9.30	37.74 \pm 11.12	43.95\pm12.63
	SF	39.47 \pm 11.15	40.98 \pm 10.84	41.26 \pm 11.59	41.76 \pm 12.48	41.41 \pm 11.76	42.34\pm12.20
	NY	41.46 \pm 11.21	42.06 \pm 11.21	47.30 \pm 13.63	41.40 \pm 12.38	42.80 \pm 13.05	57.24\pm14.23
Average (%)		54.51	54.90	57.93	54.89	56.72	61.81

C.4 Urban Feature Classification Tasks

We define six downstream classification tasks based solely on the seven non-accident features (population density and six POI densities):

dominant_poi (6-class) Identify the single most abundant POI category (office, sustenance, transportation, retail, leisure, residence) in each catchment.

poi_entropy_level (3-class) Compute the Shannon entropy of the six POI density proportions, then split into Low/Mid/High mixture levels via tertile cut.

pop_density_level (4-class) Partition population density into four quartile bins (Suburban, Inner Suburban, Urban, Core) labeled 0–3.

func_density_combo (12-class) Combine the 6 “dominant POI” classes with a binary high/low population density flag to form 12 composite categories.

nightlife_hotspot (binary) Label catchments as nightlife hotspots (1) if the leisure-to-residence POI ratio exceeds its median, else non-hotspot (0).

commercial_residential_mix (3-class) Compute the retail/(retail+residence) ratio and split into Residential-Dominant (0), Mixed (1), and Commercial-Dominant (2) via tertile cut.

Please find full results in Table 8.

Table 8: Urban POI-related tasks (%), mean \pm std). Bold indicates the best score in each city.

Task	City	DGI	InfoGraph	GCL	JOAO	SimGRACE	FractalGCL
dominant_poi	Chicago	—	—	—	—	—	—
	SF	70.74 \pm 16.14	73.13 \pm 16.27	74.23 \pm 12.35	70.88 \pm 15.31	73.97 \pm 12.97	80.75\pm12.48
	NY	45.31 \pm 15.49	47.09 \pm 14.85	49.97\pm14.56	47.08 \pm 15.78	48.27 \pm 14.97	49.42 \pm 14.90
poi_entropy_level	Chicago	36.33 \pm 9.39	38.88 \pm 10.51	38.08 \pm 12.14	35.72 \pm 10.20	38.58 \pm 11.71	39.79\pm12.32
	SF	40.21 \pm 11.09	39.30 \pm 11.13	40.00 \pm 11.77	40.01 \pm 12.86	40.48 \pm 12.21	45.48\pm13.40
	NY	37.49 \pm 10.81	36.71 \pm 10.28	37.60 \pm 12.54	35.83 \pm 11.82	36.99 \pm 12.93	40.59\pm14.02
pop_density_level	Chicago	32.91 \pm 11.00	36.42 \pm 12.07	36.97 \pm 12.75	33.11 \pm 11.41	37.44 \pm 12.75	39.55\pm13.13
	SF	47.16 \pm 12.78	49.63 \pm 12.79	50.78 \pm 12.83	46.98 \pm 12.57	51.06 \pm 12.73	51.41\pm12.80
	NY	40.09 \pm 12.61	41.35 \pm 12.77	42.17 \pm 13.06	39.77 \pm 12.72	40.75 \pm 13.42	42.76\pm13.96
func_density_combo	Chicago	—	—	—	—	—	—
	SF	50.86 \pm 13.54	53.19 \pm 12.90	55.41 \pm 12.07	51.96 \pm 13.86	55.52 \pm 11.98	58.63\pm12.46
	NY	32.41 \pm 13.14	33.18 \pm 12.95	34.84\pm12.43	33.11 \pm 13.13	34.46 \pm 12.58	34.73 \pm 12.31
nightlife_hotspot	Chicago	52.97 \pm 8.83	55.26 \pm 10.68	54.33 \pm 11.60	53.30 \pm 10.04	55.20 \pm 11.67	56.06\pm11.90
	SF	54.81 \pm 10.20	55.72 \pm 11.26	57.00 \pm 12.61	53.32 \pm 12.23	56.07 \pm 11.95	61.48\pm13.45
	NY	54.89 \pm 9.96	55.15 \pm 10.86	55.27\pm12.74	54.03 \pm 12.47	55.24 \pm 13.19	54.16 \pm 13.48
commercial_residential_mix	Chicago	37.48 \pm 9.88	37.66\pm9.93	36.98 \pm 11.48	36.93 \pm 10.52	37.05 \pm 11.26	36.59 \pm 11.71
	SF	50.14 \pm 13.74	50.35 \pm 14.31	52.74 \pm 14.27	49.61 \pm 13.81	52.94 \pm 14.32	53.01\pm14.15
	NY	37.30\pm10.69	37.17 \pm 10.95	36.96 \pm 12.65	35.93 \pm 11.98	36.53 \pm 12.90	35.92 \pm 13.17
Average	—	45.07	46.26	47.08	44.85	46.91	48.77

C.5 Conclusion

Table 7 presents the classification accuracies (mean \pm std) of six traffic-safety tasks (total-accidents-high, accident-volume-level, severity-entropy, has_sev3, has_sev4, risk_level) across Chicago, San Francisco, and New York. Table 8 reports the performance on six urban feature tasks (dominant POI, POI-entropy-level, population-density-level, function-density-combo, nightlife hotspot, commercial–residential mix) for the same set of encoders and cities. Across both tables, FractalGCL achieves the highest average accuracy and most often attains the best city–task scores.

FractalGCL consistently outperforms established contrastive baselines on both traffic-safety and urban feature classification benchmarks.

We anticipate that FractalGCL’s flexible embedding framework will extend effectively to more complex spatiotemporal and multi-modal urban analytics tasks, such as dynamic traffic flow prediction and integrated land-use and mobility modeling.